energies

MDPI

Article

Time-Domain Minimization of Voltage and Current Total Harmonic Distortion for a Single-Phase Multilevel Inverter with a Staircase Modulation

Milan Srndovic [1,*], Yakov L. Familiant [2], Gabriele Grandi [1] and Alex Ruderman [2]

[1] Department of Electrical, Electronic, and Information Engineering, University of Bologna, Viale Risorgimento 2, Bologna 40136, Italy; gabriele.grandi@unibo.it

[2] Power Electronics Research Lab, Nazarbayev University, Kabanbay Batyr Avenue 57, Astana 010000, Kazakhstan; yakov.familiant@nu.edu.kz (Y.L.F.); alexander.ruderman@nu.edu.kz (A.R.)

* Correspondence: milan.srndovic2@unibo.it; Tel.: +39-051-209-3589; Fax: +39-051-209-3588

Academic Editor: Ali Bazzi

Received: 27 July 2016; Accepted: 9 October 2016; Published: 12 October 2016

Abstract: This paper presents the optimization technique for minimizing the voltage and current total harmonic distortion (*THD*) in a single-phase multilevel inverter controlled by staircase modulation. The previously reported research generally considered the optimal *THD* problem in the frequency domain, taking into account a limited harmonic number. The novelty of the suggested approach is that voltage and current minimal *THD* problems are being formulated in the time domain as constrained optimization ones, making it possible to determine the optimal switching angles. In this way, all switching harmonics can be considered. The target function expression becomes very compact and existing efficient solvers for this kind of optimization problems can find a solution in negligible processor time. Current *THD* is understood as voltage frequency weighted *THD* that assumes pure inductive load—this approximation is practically accurate for inductively dominant RL-loads. In this study, the optimal switching angles and respective minimal *THD* values were obtained for different inverter level counts and overall fundamental voltage magnitude (modulation index) dynamic range. Developments are easily modified to cover multilevel inverter grid-connected applications. The results have been verified by experimental tests.

Keywords: multilevel inverter; staircase modulation; optimization; total harmonic distortion (*THD*)

1. Introduction

In last decades, multilevel inverters have been widely used for medium- and high-voltage/power applications [1–4]. There are many papers on this subject concerning the evaluation of either voltage or current total harmonic distortion (*THD*), typically based on voltage/current frequency spectra calculations or measurements (FFT).

In particular, the power electronics research community has recently increased its interest in voltage and current *THD* analysis for both multilevel pulse-width modulation (PWM) and staircase modulation. The analytical calculations for voltage *THD* of multilevel PWM single- and three-phase inverters have been obtained in [5] in the case of a high ratio between switching and fundamental frequencies (i.e., the so-called asymptotic approximation).

Considering pure inductive load, current *THD* actually becomes voltage frequency weighted *THD* (*WTHD*). This approximation is practically very accurate for inductively dominant RL-loads, meaning that the load time constant (L/R) is much larger than switching interval durations (in the order of half fundamental period divided by the number of levels) [6].

Much work has been done on selective harmonics elimination (SHE) techniques, described in [7–10]. However, although SHE techniques can totally eliminate certain low-order harmonics, they do not have a minimization impact on either voltage or current *THD*, taking into account all harmonics.

To evaluate and optimize multilevel voltage/current quality, the research community typically uses a limited harmonics count (51, as recommended by Institute of Electrical and Electronics Engineers (IEEE) Standard 519 [11] or others, like 101) that causes the underestimation of *THD* [12,13].

Recently, there have not been so many developments where the infinite harmonic content is taken into account for the voltage and current quality estimation in multilevel inverters. One reason might be a generally high complexity of a possible mathematical approach or the fact that sometimes there is no practical need to consider infinitely many harmonics. Recent publications have shown that it is quite feasible to consider an infinite harmonic content for the voltage *THD* when making multilevel voltage waveform analysis in the time domain [14–16]. Optimal switching angles that minimize single-phase multilevel inverter voltage *THD* for a given level count are presented in [15] and [16] without explicitly indicating the corresponding modulation index.

This paper presents the analysis and experimental verification of voltage and current *THD* minimization problems for a single-phase multilevel inverter over the whole modulation index range, using the time-domain problem formulations preliminarily introduced in [17]. Voltage *THD* optimization results of [15,16] are included as a special case. Based on the authors' knowledge, the breakthrough of the proposed method is a current quality optimization and minimization for multilevel single-phase inverters using the time-domain *WTHD* taking into consideration all possible switching harmonics.

Comparing the proposed time-domain (*W*)*THD* method with the standard frequency-domain *THD* minimization for voltage and current brings some advantages, such as results equivalent to unlimited harmonics content, avoiding Fourier trigonometric calculation of large number of harmonic magnitudes, reduced processor time, and reduced accumulated numerical errors. In this case, the only calculation based on the frequency domain is the Fourier calculation to determine the amplitude of a fundamental component (i.e., the modulation index), which is unavoidable.

The paper is organized as follows. In Section 2, general expressions for fundamental voltage and current mean square approximation errors and *THD* are derived. Voltage and current *THD* minimization problems are formulated as time-domain constrained optimization ones. In Section 3, minimal voltage and current *THD* solutions by numerically constrained optimization are presented and discussed. While Section 3 considers current *THD* for inductively dominant RL-load, current *THD* calculation in the case of the grid connection is discussed in Section 4. The verification of theoretical results, carried out by Matlab–Simulink simulations and laboratory experiments, is presented in Section 5. Conclusions are given in Section 6.

2. Optimal Voltage and Current Quality Time-Domain Problem Formulation

In order to obtain minimal voltage and current *THD*s, it is necessary to find optimal switching angles that minimize mean square approximation error. The problem formulation in a frequency domain, as a general optimization which considers a limited harmonic count, is a possible source of inaccuracy [12,13,18]. To find an optimal solution which considers all harmonics, the optimization problem must be formulated in a time domain, and as a constrained optimization one.

Figure 1 gives an example of cascaded H-bridge single-phase inverter with n = 1, 2, and 3 cells, and the output voltage waveforms (half-waves) in the case of staircase modulation with five and seven output voltage levels. Due to quarter-wave symmetry, there are two and three independent switching angles, respectively. Current waveforms (half-waves) are obtained by time integration of the voltage waveforms that assumes pure inductive (or inductively dominant) load.

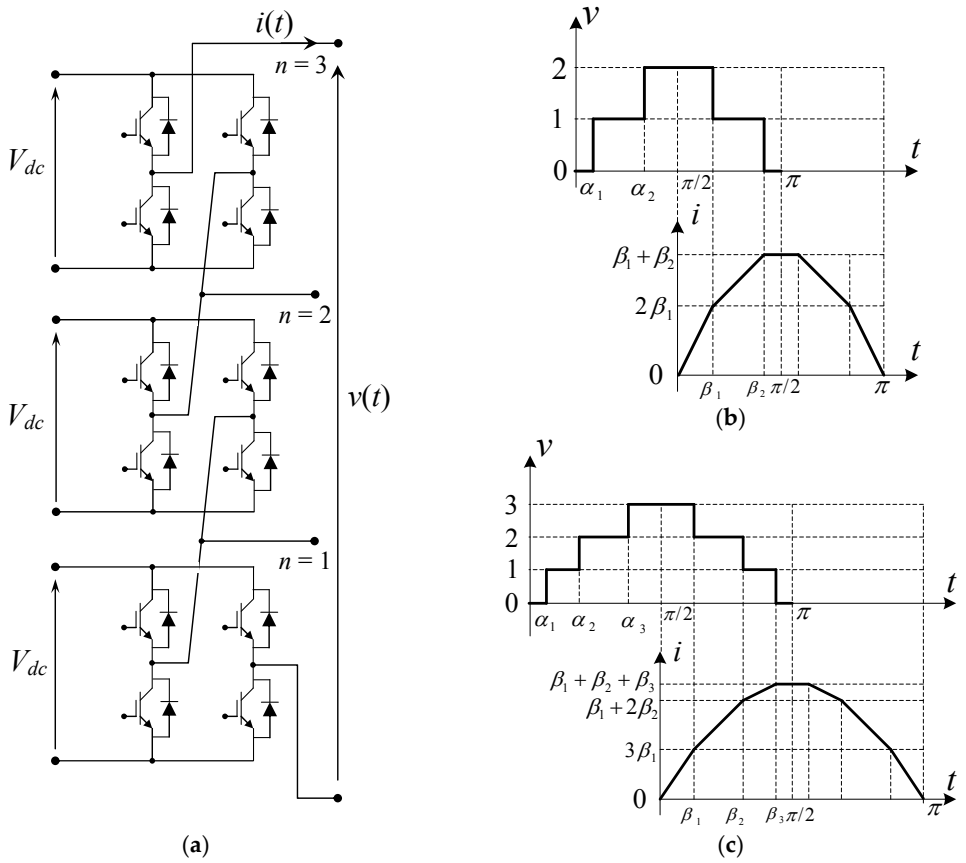

Figure 1. (**a**) Cascaded H-bridge inverter (n = 1, 2, 3): voltage and current half-waves (p.u.) for staircase modulation in case of (**b**) five levels and (**c**) seven levels.

A precise closed-form expression for voltage (current) approximation error normalized mean square (voltage ripple *NMS* [5]) may be obtained by integrating the squared (normalized) voltage waveform average following a quarter-wave symmetry, as Equation (1):

$$NMS_V(m) = \frac{2}{\pi}\int_0^{\pi/2} v^2(\tau)\,\mathrm{d}\tau - \frac{1}{2}m^2 \tag{1}$$

For a two-cell inverter (n = 2) with five-level voltage waveform (Figure 1b), the modulation index m, using the direct Fourier series fundamental term calculation, is Equation (2):

$$m = \frac{4}{\pi}\int_{\alpha_1}^{\alpha_2} \sin(\alpha)\mathrm{d}\alpha + \frac{4}{\pi}\int_{\alpha_2}^{\pi/2} 2\sin(\alpha)\mathrm{d}\alpha = \frac{4}{\pi}[\cos(\alpha_1) + \cos(\alpha_2)] \tag{2}$$

The expression for the voltage approximation mean square error to be minimized becomes Equation (3):

$$NMS_V^2(m,\alpha_1,\alpha_2) = \frac{2}{\pi}\int_{\alpha_1}^{\alpha_1} \mathrm{d}\alpha + \frac{2}{\pi}\int_{\alpha_2}^{\pi/2} 2^2\mathrm{d}\alpha - \frac{1}{2}m^2 = 4 - \frac{2}{\pi}(\alpha_1 + 3\alpha_2) - \frac{1}{2}m^2 \tag{3}$$

Additionally, the switching angles limitations are Equation (4):

$$0 < \alpha_1 < \arcsin\left(\frac{1}{m}\right), \quad \arcsin\left(\frac{1}{m}\right) < \alpha_2 < \pi/2 \tag{4}$$

For a three-cell inverter (n = 3) with seven-level voltage waveform (Figure 1c), the modulation index m and mean square error are Equations (5) and (6):

$$m = \frac{4}{\pi}[\cos(\alpha_1) + \cos(\alpha_2) + \cos(\alpha_3)], \tag{5}$$

$$NMS_V^3(m, \alpha_1, \alpha_2, \alpha_3) = 9 - \frac{2}{\pi}(\alpha_1 + 3\alpha_2 + 5\alpha_3) - \frac{1}{2}m^2 \tag{6}$$

In this case, switching angle limitations are similar to Equation (4).

For an arbitrary cell count n (n switching angles and $2n + 1$ voltage levels), modulation index becomes Equation (7):

$$m = \frac{4}{\pi}\sum_{k=1}^{n}\cos(\alpha_k) \tag{7}$$

and voltage ripple *NMS* is Equation (8):

$$NMS_V^n(m, \alpha_1, \ldots, \alpha_n) = n^2 - \frac{2}{\pi}\sum_{k=1}^{n}(2k-1)\alpha_k - \frac{1}{2}m^2 \tag{8}$$

Using the frequency domain definition, voltage *THD* expression is determined using Equation (9):

$$THD_V(m), \% = \frac{\sqrt{\sum_{k=2}^{\infty} V_k^2}}{V_1} \cdot 100 \tag{9}$$

The relationship between voltage ripple *NMS* and voltage *THD*, due to Parseval's theorem (Rayleigh energy theorem), can be written as Equation (10):

$$THD_V^n(m), \% = \frac{\sqrt{2NMS_V^n(m)}}{m} \cdot 100 \tag{10}$$

For a given modulation index m, the voltage *THD* optimization problem is formulated as a constrained optimization one with *THD* in Equation (10) (*NMS* in Equation (8)) as a target function to be minimized, modulation index in Equation (7) as an equality constraint, and staircase modulation-imposed limitations on switching angles similar to Equation (4) as inequality constraints.

The challenge of a time-domain current *THD* analysis in pure inductive load approximation (voltage *WTHD*), as Equation (11):

$$WTHD_V(m), \% = THD_I(m), \% = \frac{\sqrt{\sum_{k=2}^{\infty}\left(\frac{V_k}{k}\right)^2}}{V_1} \cdot 100 \tag{11}$$

is finding closed-form expressions for current approximation mean square error for piecewise linear (normalized) current waveforms obtained by time integration of their respective voltage waveforms (Figure 1b,c).

For Figure 1, the normalized current analysis for the pure inductive load, which assumes both normalized fundamental angular frequency and load inductance equal unity, fundamental current harmonic magnitude equals voltage modulation index m.

Then, current ripple *NMS* may be calculated, similar to Equation (1), by calculating the (normalized) squared current waveform average on a quarter-wave interval.

For two and three angles, by direct current mean square value computation, current ripple *NMS* is found using Equation (12):

$$NMS_I^2(m,\beta_1,\beta_2) = (\beta_1+\beta_2)^2 - \frac{\frac{6}{3}\beta_1^3+\frac{4\beta_2^3}{3}+2\beta_1\beta_2^2}{\pi} - \frac{1}{2}m^2$$
$$\beta_1 = \pi/2-\alpha_2, \quad \beta_2 = \pi/2-\alpha_1, \tag{12}$$

$$NMS_I^3(m,\beta_1,\beta_2,\beta_3) = (\beta_1+\beta_2+\beta_3)^2 - \frac{\frac{8\beta_1^3}{3}+\frac{6}{3}\beta_2^3+\frac{4\beta_3^3}{3}+2(\beta_1\beta_2^2+\beta_1\beta_3^2+\beta_2\beta_3^2)}{\pi} - \frac{1}{2}m^2$$
$$\beta_1 = \pi/2-\alpha_3,\ \beta_2 = \pi/2-\alpha_2,\ \beta_3 = \pi/2-\alpha_1. \tag{13}$$

For an arbitrary cell count n (n = switching angles, and $2n+1$ = voltage levels), the general current *NMS* formula becomes Equation (14):

$$NMS_I^n(m,\beta_1,\ldots,\beta_n) = \left(\sum_{k=1}^{n}\beta_k\right)^2 - \frac{2}{\pi}\left[\frac{1}{3}\sum_{k=1}^{n}(n+2-k)\,\beta_k^3 + \sum_{k=1}^{n-1}\left(\beta_k\sum_{i=k+1}^{n}\beta_i^2\right)\right] - \frac{1}{2}m^2$$
$$\beta_k = \pi/2-\alpha_{n-k+1},\ k=1,2,\ldots,n. \tag{14}$$

To derive *NMS* in Equations (12)–(14), Matlab symbolic calculations were used because manual computations become too burdensome starting from three cells (three angles).

3. Optimal Voltage and Current Total Harmonic Distortion Solutions

The constrained *THD* (*NMS*) minimization problems with modulation index equality and switching angles inequality constraints described in the previous section are effectively solved by means of Matlab function *fmincon*. Voltage and current optimization solutions for a single-phase five-cell multilevel inverter (up to 5 angles and 11 voltage levels) are shown in Figures 2–5.

Over the interlevel modulation index intervals 1–2, 2–3, 3–4, 4–5, voltage and current quadratic approximation error (*NMS*/*THD*) local minima and maxima appear. Global voltage *THD* minima found in [15,16] for up to 6–7 angles without explicitly indicating the modulation indices are, in fact, local minima of voltage *THD* curve in Figure 2.

Voltage and current optimal switching angles might be considerably different (Figures 4 and 5), and current angles' curves are much smoother. Over each interlevel interval, there are two working points at which voltage *THD* optimal angles and current *THD* (voltage *WTHD*) optimal angles are identical, having the same modulation index. Regarding the aforesaid, for the selected modulation indexes the voltage and current *THD*s are minimal.

Figure 2. Minimal voltage total harmonic distortion (*THD*) for n = 5 (up to 11 voltage levels).

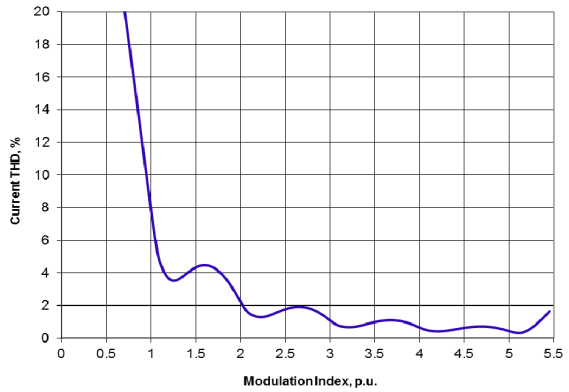

Figure 3. Minimal current *THD* for $n = 5$ (up to 11 voltage levels).

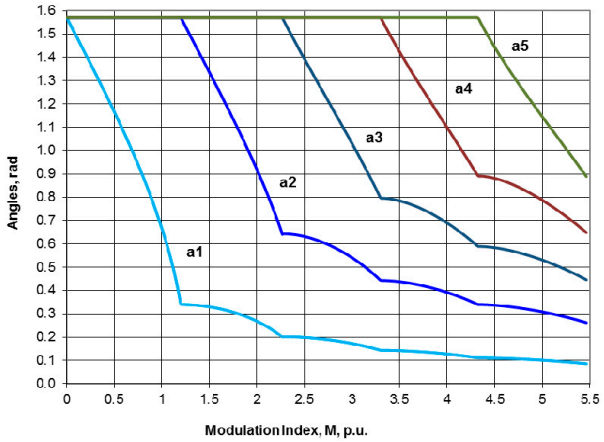

Figure 4. Voltage optimal switching angles for $n = 5$ (up to 11 voltage levels).

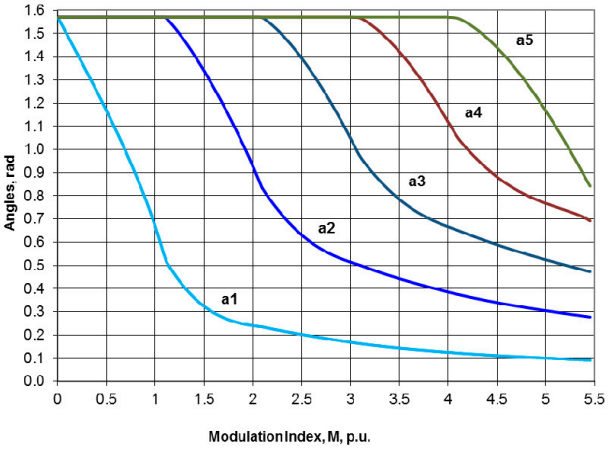

Figure 5. Current optimal switching angles for $n = 5$ (up to 11 voltage levels).

Sensitivity study shows that optimal current *THD* is much more susceptible to switching angles variations compared with optimal voltage *THD*. The low susceptibility to angles variations of optimal voltage *THD* is known from the previous research [12,13]. On the whole, a coarse piecewise constant optimal approximation is very robust from possible disturbances point of view, such as angle/level variations and rounding errors.

Comparing the optimal voltage and current *THD*s, the current *THD* is much more susceptible to switching-angles variations. This happens due to the fact that a supposed fine piecewise linear optimal

approximation (compared to a coarse piecewise constant one) is more susceptible in terms of possibly being affected by some disturbances.

Making a comparison between optimal voltage and current *THD* (Figures 2 and 3), it might be seen that current *THD* curve ripple is much larger considering the noticeable difference between adjacent maxima and minima in the order of 100%. This leads to the fact that current *THD* may be essentially reduced just by selecting a proper converter working point (modulation index) selection. On the contrary, there might be a significant current *THD* increase as a penalty for a detuned operation.

Regarding Figures 2 and 3, note that the curve of *THD* average trend can be approximated by simple hyperbolic approximations [17].

4. Current Total Harmonic Distortion for a Grid-Connected Inverter

The previous analysis aims at current *THD* for pure inductive loads (voltage *WTHD*) and the results are practically applicable to inductively dominant RL-loads. A similar analysis can be carried out for a grid-connected inverter application as well (Figure 6), considering a link inductor.

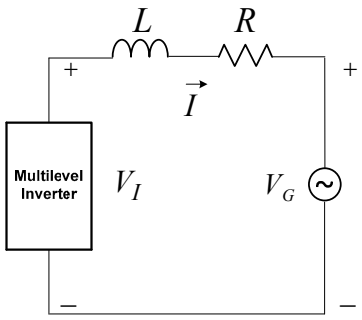

Figure 6. Single-phase multilevel inverter connected to the single-phase grid by a link inductor.

In order to have maximum transferred power to the electrical grid at a given magnitude of the grid current, the current has to be in phase with the corresponding grid voltage, as it is depicted by the phasor diagram in Figure 7.

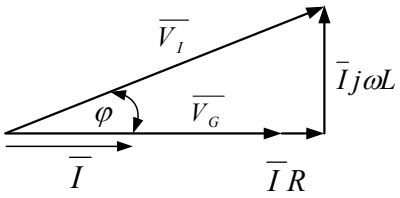

Figure 7. Phasor diagram for maximum transferred power.

According to Figure 7, inverter voltage parameters become:

$$V_I = \sqrt{(V_G + IR)^2 + (I\omega L)^2} \tag{15}$$

$$\phi = \arctan\left(\frac{I\omega L}{V_G + IR}\right) \tag{16}$$

For the link inductor, the resistive part in Equations (15) and (16) can be neglected (i.e., $\omega L >> R$), leading to:

$$V_I = \sqrt{{V_G}^2 + (I\omega L)^2} \tag{17}$$

$$\phi = \arctan\left(\frac{I\omega L}{V_G}\right) \tag{18}$$

For grid-connected applications, voltage modulation index for zero current can be defined as Equation (19):

$$m_G = \frac{V_G}{V_{dc}} \tag{19}$$

Then, modulation index:

$$m = \sqrt{{m_G}^2 + \left(\frac{I\omega L}{V_{dc}}\right)^2} \tag{20}$$

where V_{dc} is the converter dc bus voltage (expected of the order of 0.7–0.8 half-waves (p.u.)), V_G is the grid voltage, and I is the current magnitude. Current THD then becomes Equation (21):

$$THD_I = \sqrt{\frac{2NMS_I(m)}{m^2 - m_G^2}} = \frac{V_{DC}}{I\omega L}\sqrt{2NMS_I(m)} \approx \frac{V_{DC}}{I\omega L}\sqrt{2NMS_I(m_G)} \tag{21}$$

5. Laboratory Verification

Experimental verifications were performed for a single-phase cascaded H-bridge inverter having three properly connected H-bridge cells ($n = 3$), each one with the individual dc bus voltage $V_{dc} = 200$ V, according to Figure 1a,c. The circuit scheme of the experimental setup and the workbench are shown in Figures 8 and 9.

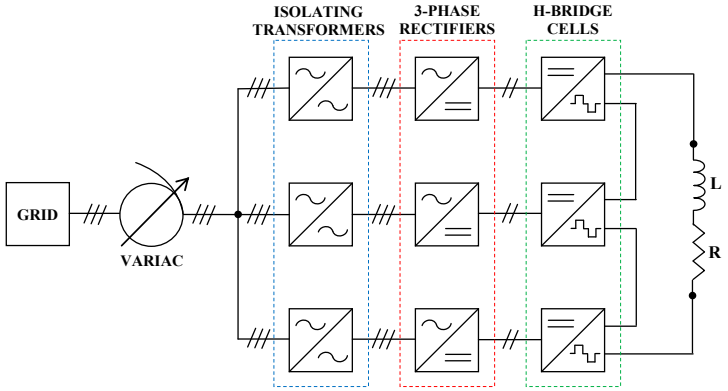

Figure 8. Circuit scheme of the experimental setup.

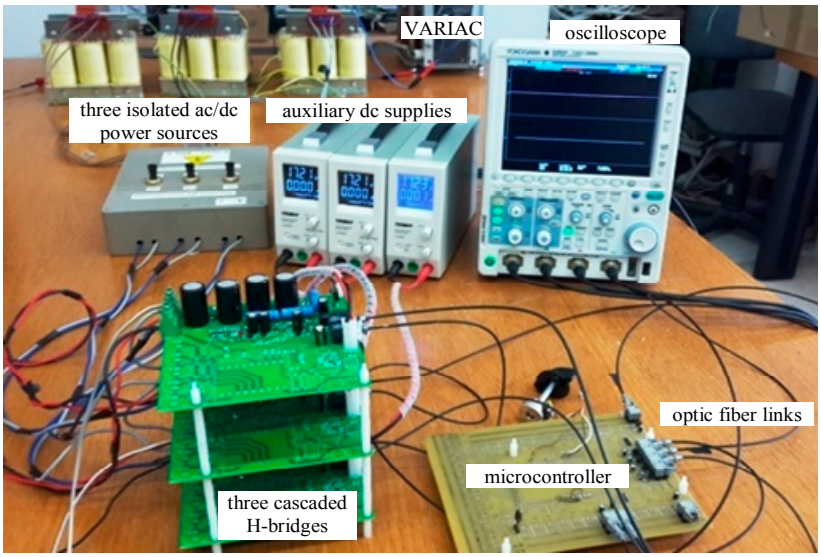

Figure 9. Experimental workbench.

It consists of three 3x Mitsubishi power IGBT modules IPM PS22A76 (1200 V, 25 A, Mitsubishi Electric Corporation, Tokyo, Japan), controlled by "Arduino Due" microcontroller board (84 MHz Atmel, SAM3X83 Cortex-M3 CPU, Somerville, MA, USA). The signal measuring equipment includes the PICO TA057 differential voltage probe (25 MHz, ±1400 V, ±2%, Pico Technology, Tyler, TX, USA) and LEM PR30 current probe (dc to 20 kHz, ±20 A, ±1%, LEM Europe GmbH, Fribourg, Switzerland) connected to the Yokogawa DLM 2024 oscilloscope (Yokogawa Electric Corporation, Tokyo, Japan). The LCR meter Agilent 4263B (Santa Rosa, CA, USA) was used to obtain the passive RL-load parameters, L = 481 mH, R = 24.7 Ω, measured at 100 Hz.

Minimal voltage and current *THD* curves within the modulation index range for such inverter configuration (n = 3, up to 7 voltage levels) are shown in Figures 10 and 11. Voltage and current optimal switching angles are given in Figure 12 (current angle curves are the smoother ones). Considering these figures, the six working conditions indicated by dots were chosen for the experimental tests. In particular, two test points (a) and (b) have been selected for minimum and maximum values of voltage and current *THD*s over the modulation index range corresponding to seven levels, respectively (Figures 10 and 11). Furthermore, two test points (a) and (b) have been selected corresponding to the modulation index m when both voltage and current have the optimal values of *THD* for the same three switching angles (Figure 12).

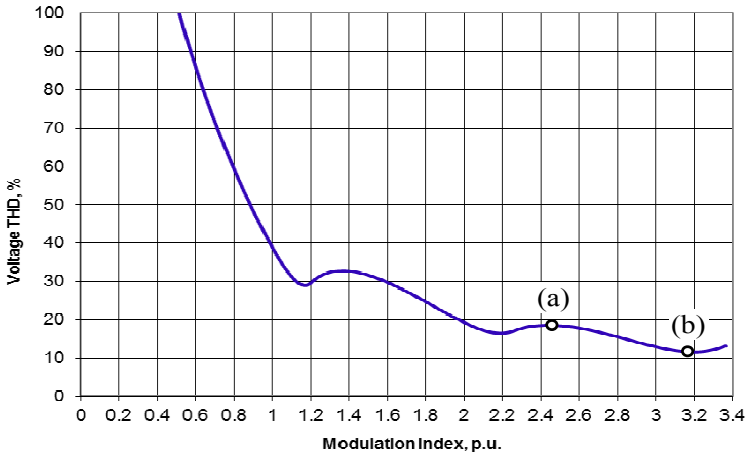

Figure 10. Minimal voltage *THD* vs. modulation index for n = 3.

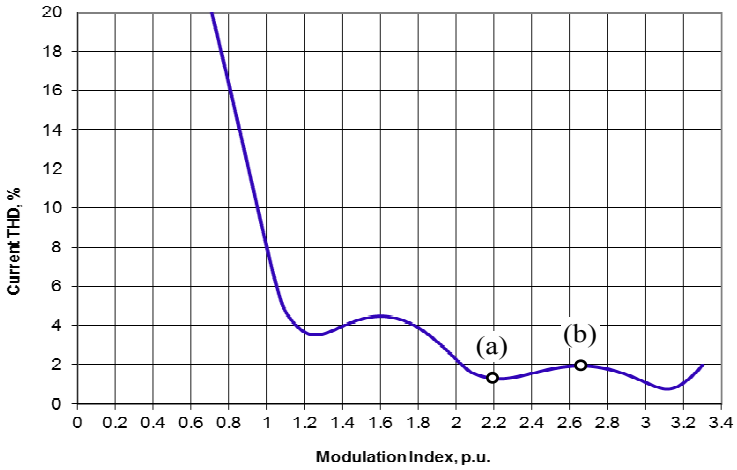

Figure 11. Minimal current *THD* vs. modulation index for n = 3.

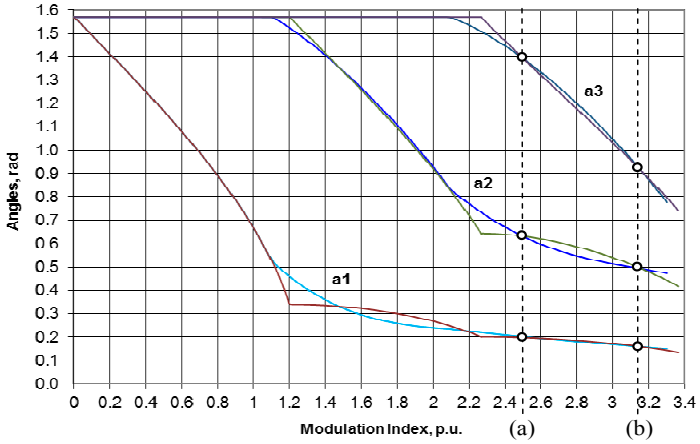

Figure 12. Voltage and current optimal switching angles for $n = 3$.

In Figures 13–15, the corresponding experimental results are presented, showing the test points (a) and (b). All figures depict the waveforms over the 2.5 fundamental periods. Due to limited scope functions, it is not possible to directly display full legends on screenshots. What can be noticed is that on the top of each screenshot the scales of waveforms are displayed with the colors which correspond to the waveform colors. Also, on the left side of all screenshots there are full-range scales with the same colors. The description of those waveforms is given in the first half of Table 1: load voltage (blue trace)—scope channel 2, labeled C2 (CH2), load current (red trace)—scope channel 3, labeled C3 (CH3), the top half screen; fundamental of load voltage (purple trace), labeled M1, and voltage ripple (green trace), labeled M2: CH2 − M1, are depicted in the bottom half screen of Figures 13 and 15; fundamental of load current (orange trace), labeled M1 and current ripple (green trace, magnified by 4), labeled M2: CH3 − M1, are depicted in the bottom half screen of Figures 14 and 15. It should be noted that while calculating the voltage *THD*, mathematical functions M1 and M2 are applied the load voltage waveform, and while calculating the current *THD* they are applied to the load current waveform.

Fundamental components have been determined by built-in scope infinite impulse response (IIR) filter function (M1), and ripple components have been calculated as the difference between the actual waveforms and the corresponding fundamental components (M2 = CH2(3) − M1). *THD*s have been determined as the ratio between ripple root mean square (*RMS*) and fundamental *RMS*. Specific calculation of *RMS* and *THD* for all voltage and current waveforms have been carried out by the scope built-in advanced mathematical functions in real time and displayed on the bottom lines of the scope screen. Corresponding designations with the calculation of voltage (current) *THD* are presented in the last part of Table 1.

Table 1. Waveforms' parameters calculated by the scope built-in advanced mathematical functions. RMS: root mean square.

Label	Description	Signal Waveforms and Calculated Parameters
C2	Scope channel 2, CH2	Load voltage
C3	Scope channel 3, CH3	Load current
M1	Math function 1: IIR low pass filter	Fundamental voltage (current)
M2	Math function 2: CH2 (CH3) − M1	Ripple voltage (current)
Rms(C2)	Math function RMS on CH2	Total voltage *RMS*
Rms(C3)	Math function RMS on CH3	Total current *RMS*
Calc2	Built-in math calculation 2	Fundamental voltage (current) *RMS*
Calc3	Built-in math calculation 3	Ripple voltage (current) *RMS*
Calc4	Built-in math calculation 4	Voltage (current) *THD*% calculated as: $THD_{V(I)}, \% = \frac{Rms(\mathrm{M2})}{Rms(\mathrm{M1})} \cdot 100$

Figure 13 presents two cases for local maximum and minimum values of the voltage *THD* over the considered modulation index range. Figure 13a corresponds to the case of local max V_{THD} for $m = 2.459$ ($\alpha_1 = 0.119$, $\alpha_2 = 0.635$, $\alpha_3 = 1.424$), while Figure 13b corresponds to the case of local min V_{THD} for $m = 3.194$ ($\alpha_1 = 0.155$, $\alpha_2 = 0.482$, $\alpha_3 = 0.884$).

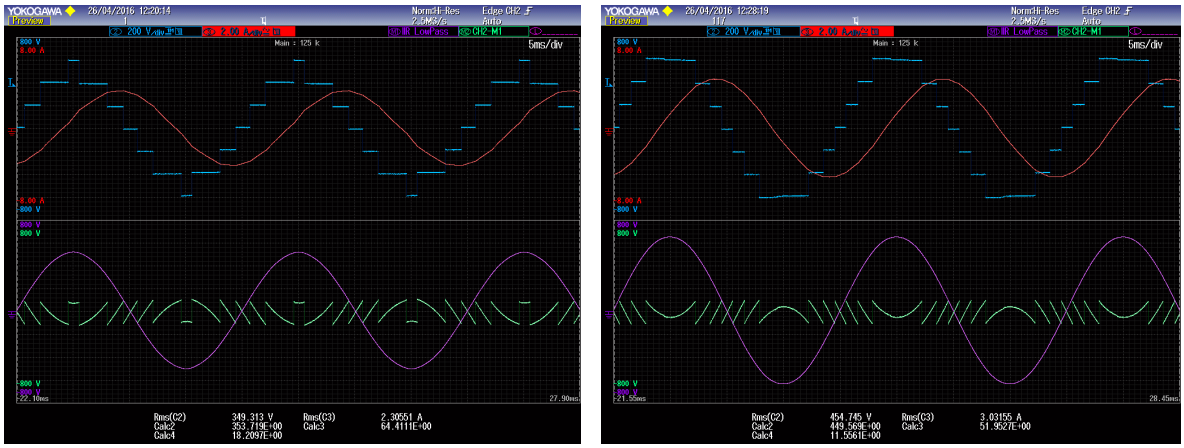

(**a**) (**b**)

Figure 13. Minimized voltage *THD* (Figure 10): (**a**) $m = 2.45$ ($\alpha_1 = 0.119$, $\alpha_2 = 0.635$, $\alpha_3 = 1.424$); and (**b**) $m = 3.19$ ($\alpha_1 = 0.155$, $\alpha_2 = 0.482$, $\alpha_3 = 0.884$).

Figure 14 presents two cases for local minimum and maximum values of the current *THD* over the considered modulation index range. Figure 14a corresponds to the case of local min I_{THD} for $m = 2.221$ ($\alpha_1 = 0.224$, $\alpha_2 = 0.758$, $\alpha_3 = 1.527$), while Figure 14b corresponds to the case of local max I_{THD} for $m = 2.663$ ($\alpha_1 = 0.190$, $\alpha_2 = 0.580$, $\alpha_3 = 1.294$).

(**a**) (**b**)

Figure 14. Minimized current *THD* (Figure 11): (**a**) $m = 2.22$ ($\alpha_1 = 0.224$, $\alpha_2 = 0.758$, $\alpha_3 = 1.527$); and (**b**) $m = 2.66$ ($\alpha_1 = 0.190$, $\alpha_2 = 0.580$, $\alpha_3 = 1.294$).

Figure 15 considers the cases of two modulation indices where optimal voltage *THD* and optimal current *THD* occur for the same switching angles, over the considered modulation index range. Figure 15a corresponds to the case $m = 2.494$ ($\alpha_1 = 0.202$, $\alpha_2 = 0.633$, $\alpha_3 = 1.397$), while Figure 15b corresponds to the case $m = 3.144$ ($\alpha_1 = 0.160$, $\alpha_2 = 0.495$, $\alpha_3 = 0.925$).

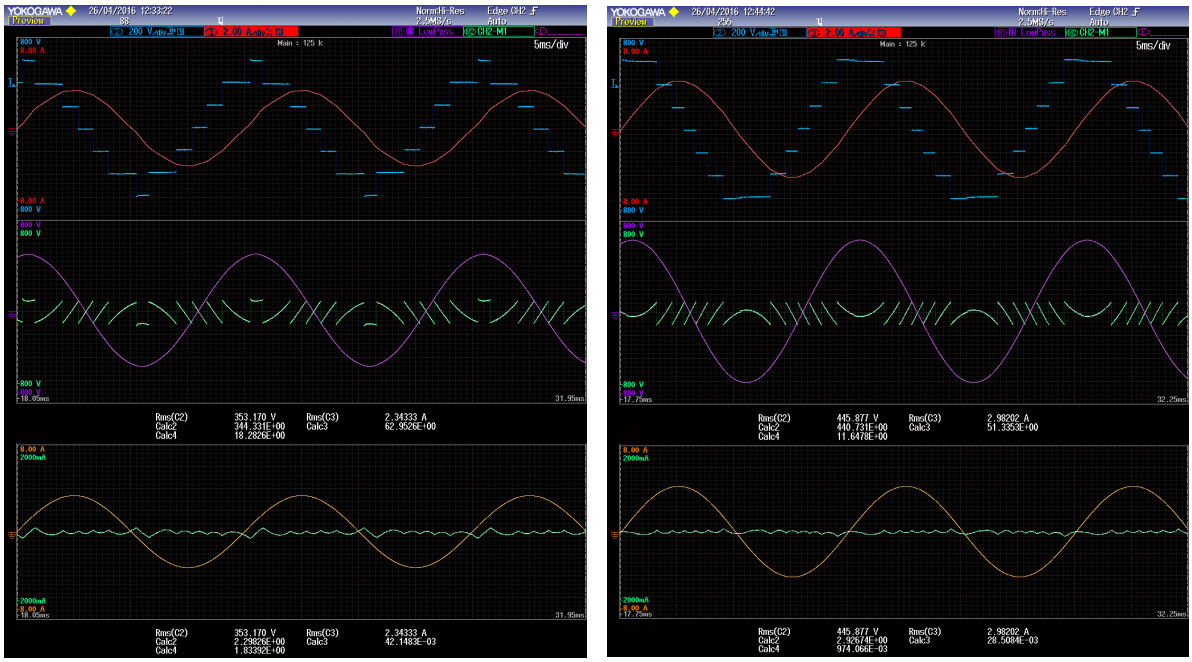

(**a**) (**b**)

Figure 15. Minimized voltage and current *THD*s (Figure 12): (**a**) $m = 2.49$ ($\alpha_1 = 0.202$, $\alpha_2 = 0.633$, $\alpha_3 = 1.397$); and (**b**) $m = 3.14$ ($\alpha_1 = 0.160$, $\alpha_2 = 0.495$, $\alpha_3 = 0.925$).

The experimental results (*Exp.*) are summarized in Tables 2 and 3, and compared with both theoretical calculations (*Calc.*) and simulation results (*Sim.*, obtained by Matlab–Simulink).

Table 2. Minimized voltage and current *THD*s—specific cases.

Test Point	Minimized THD_V (%)				Minimized THD_I (%)			
	m	*Calc.*	*Sim.*	*Exp.*	*m*	*Calc.*	*Sim.*	*Exp.*
(a)	2.45	18.50	18.49	18.21	2.22	1.29	1.31	1.43
(b)	3.19	11.53	11.52	11.55	2.66	1.93	1.96	2.03

Table 3. Minimized voltage and current *THD*s—same switching angles.

Test Point	Both	Minimized THD_V (%)			Minimized THD_I (%)		
	m	*Calc.*	*Sim.*	*Exp.*	*Calc.*	*Sim.*	*Exp.*
(a)	2.49	18.43	18.59	18.28	1.54	1.56	1.83
(b)	3.14	11.65	11.64	11.65	0.81	0.82	0.97

Table 2 presents the four cases corresponding to Figure 13a,b and Figure 14a,b. It can be noticed that calculated, simulated, and experimental *THD*% values have a really good matching in the case of minimized voltage *THD* (left table side). In the case of current *THD* (right table side), calculated values match the simulation ones, and the experimental values are slightly higher due to the really small values of the current ripple, which emphasize the measuring errors such as current probe errors and inverter nonlinearities (switching losses, dead-times, etc). Corresponding slight errors have been observed introducing similar nonidealities in the simulation tests.

Table 3 presents two cases (a) and (b) of Figure 15, where the same three switching angles result for optimizing both the voltage and the current *THD*s, corresponding to the same modulation index, as shown in Figure 12. As expected, the experimental voltage *THD* results match almost perfectly both

theoretical and simulated results, while the current *THD* results have slightly higher values, due to similar aforementioned reasons.

In general, the very slight difference between (ideal) simulations and calculated theoretical results in case of current *THD* can be justified, considering that the considered load is not pure inductive. In the specific test cases, the load impedance angle is about 81°, a bit lower than the theoretical angle of 90°. This is introducing a more than acceptably small error due to the high current *THD* sensitivity, proving the effectiveness of the assumption of inductively dominant load. On the whole, simulation and experimental results match the supposed ones in a satisfactory way.

6. Conclusions

Minimal voltage and current *THD* for a single-phase multilevel inverter with uniformly distributed voltage levels are formulated as constrained optimization ones in a time domain, considering all switching harmonics. Current *THD* is considered in a pure inductive load approximation (corresponding to voltage frequency weighted *THD*, *WTHD*). Comparing with minimal voltage *THD* time-domain problem formulations which have been reported previously, the minimal current *THD* time-domain problem formulation is a novel one. It becomes feasible due to analytical closed-form symbolic calculations of piecewise linear current waveform mean squares.

The numerical solutions establish theoretical calculation of voltage and current *THD* lower bounds for a single-phase multilevel inverter with a staircase modulation. Optimal switching angles and minimal voltage and current *THD*s are reported for different multilevel inverter cell numbers (different voltage level counts) and overall modulation index dynamic range. All calculations for optimal switching angles are quite simple and require a negligible processor time due to the fact that they can be easily calculated offline and called from the microcontroller memory. Also, every microcontroller can perform a simple linear interpolation, so high accuracy of the modulation index is not needed and, therefore, neither is its real-time calculation.

Over every interlevel modulation index interval, there are two working points which present the set of switching angles where the optimal voltage and current *THD* are achieved. Modulation indexes which correspond to those two working points are so-called twice optimal modulation indices.

It is shown that optimal voltage *THD* solutions have relatively low sensitivity to switching angles variations and other disturbances. On the other hand, sensitivity of current optimal solutions is relatively high due to a fine piecewise linear optimal approximation which is much more susceptible to possible disturbances compared with a coarse piecewise constant optimal one.

In the case of grid-connected applications, normalized current fundamental harmonic is typically about 10 times smaller than the voltage modulation index. Following this, the *THD* value of the grid-connected current increases in the same proportion, due to the direct proportion between the current *THD* and the normalized current magnitude, compared with the case when there is an inductively dominant load. This comparison is valid for the same modulation indexes for both practical cases. It is shown that only about 10% modulation index variations might cause around 100% of current *THD* changes. Considering this, there is a space for examining the optimal working point from the point of view of the minimal current *THD* values, and controlling in parallel the dc bus and grid voltage variations.

Theoretical findings are solidified by computer simulations and a wide set of laboratory verification. Experimental results confirm the correctness of the proposed mathematical approach for pure inductively dominant load for voltage and current *THD* calculations.

Acknowledgments: This research was funded under the Target Program 0115PK03041 "Research and development in the fields of energy efficiency and energy saving, renewable energy sources and environmental protection" for years 2014–2016 from the Ministry of Education and Science of the Republic of Kazakhstan.

Author Contributions: All the contributions in this paper are equally shared among the authors Milan Srndovic, Yakov L. Familiant, Gabriele Grandi and Alex Ruderman.

Conflicts of Interest: The authors declare no conflict of interest.

References

1. Rodríguez, J.; Bernet, S.; Wu, B.; Pontt, J.O.; Kouro, S. Multilevel voltage-source-converter topologies for industrial medium-voltage drives. *IEEE Trans. Ind. Electron.* **2007**, *54*, 2930–2945. [CrossRef]
2. Buticchi, G.; Barater, D.; Lorenzani, E.; Concari, C.; Franceschini, G. A nine-level grid-connected converter topology for single-phase transformerless PV systems. *IEEE Trans. Ind. Electron.* **2014**, *61*, 3951–3960. [CrossRef]
3. Tarisciotti, L.; Zanchetta, P.; Watson, A.; Bifaretti, S.; Clare, J.C. Modulated model predictive control for a seven-level cascaded H-bridge back-to-back converter. *IEEE Trans. Ind. Electron.* **2014**, *61*, 5375–5383. [CrossRef]
4. Mora, A.; Lezana, P.; Juliet, J. Control scheme for an induction motor fed by a cascade multicell converter under internal fault. *IEEE Trans. Ind. Electron.* **2014**, *61*, 5948–5955. [CrossRef]
5. Ruderman, A.; Reznikov, B.; Busquets-Monge, S. Asymptotic time domain evaluation of a multilevel multiphase PWM converter voltage quality. *IEEE Trans. Ind. Electron.* **2013**, *60*, 1999–2009. [CrossRef]
6. Holmes, G.D.; Lipo, T.A. *Pulse Width Modulation for Power Converters: Principles and Practice*; Wiley-IEEE Press: Oxford, UK, 2003.
7. Chiasson, J.; Tolbert, L.M.; Mckenzie, K.; Du, Z. Elimination of Harmonics in a Multilevel Converter Using the Theory of Symmetric Polynomials and Resultants. In Proceedings of the 42nd IEEE Conference on Decision and Control, Maui, HI, USA, 9–12 December 2003.
8. Du, Z.; Tolbert, L.M.; Chiasson, J.; Ozpineci, B. Reduced switching-frequency active harmonic elimination for multilevel converters. *IEEE Trans. Ind. Electron.* **2008**, *55*, 1761–1770.
9. Buccella, C.; Cecati, C.; Cimoroni, M.G.; Razi, K. Analytical method for pattern generation in five-level cascaded H-Bridge inverter using selective harmonic elimination. *IEEE Trans. Ind. Electron.* **2014**, *61*, 5811–5819. [CrossRef]
10. Dahidah, M.S.A.; Konstantinou, G.; Agelidis, V.G. A review of multilevel selective harmonic elimination PWM: Formulations, solving algorithms, implementation and applications. *IEEE Trans. Ind. Electron.* **2015**, *30*, 4091–4106. [CrossRef]
11. *IEEE Recommended Practices and Requirements for Harmonic Control in Electrical Power Systems*; American National Standard (ANSI); Institute of the Electrical and Electronics Engineering Inc.: New York, NY, USA, 1993.
12. Diong, B. THD-optimal staircase modulation of single-phase multilevel inverters. In Proceedings of the 2006 IEEE Region 5 Conference, San Antonio, TX, USA, 7–9 April 2006.
13. Diong, B.; Sepahvand, H.; Corzine, K.A. Harmonic distortion optimization of cascaded H-Bridge inverters considering device voltage drops and noninteger DC voltage ratios. *IEEE Trans. Ind. Electron.* **2013**, *60*, 3106–3114. [CrossRef]
14. Alberto, C.; Espinosa, L.; Portocarrero, I.; Izquierdo, M. Minimization of THD and angle calculation for multilevel inverters. *Int. J. Eng. Technol.* **2012**, *5*, 83–86.
15. Luo, L.F. Investigation on best switching angles to obtain lowest THD for multilevel DC/AC inverters. In Proceedings of the 2013 8th IEEE Conference on the Industrial Electronics and Applications (ICIEA), Melbourne, Australia, 19–21 June 2013.
16. Espinosa, E.E.; Espinoza, J.R.; Melín, P.E.; Ramírez, R.O.; Villarroel, F.; Muñoz, J.A.; Morán, L. A new modulation method for a 13-Level asymmetric inverter toward minimum THD. *IEEE Trans. Ind. Appl.* **2014**, *50*, 1924–1933. [CrossRef]
17. Koishybay, K.; Familiant, Y.L.; Ruderman, A. Minimization of Voltage and Current Total Harmonic Distortion for a Single-Phase Multilevel Inverter Staircase Modulation. In Proceedings of the 2015 9th International Conference on Power Electronics and ECCE Asia (ICPE-ECCE Asia), Seoul, Korea, 1–5 June 2015.
18. Roberge, V.; Tarbouchi, M.; Okou, F. Strategies to accelerate harmonic minimization in multilevel inverters using a parallel genetic algorithm on graphical processing unit. *IEEE Trans. Power Electron.* **2014**, *29*, 5087–5090. [CrossRef]

© 2016 by the authors; licensee MDPI, Basel, Switzerland. This article is an open access article distributed under the terms and conditions of the Creative Commons Attribution (CC-BY) license (http://creativecommons.org/licenses/by/4.0/).